Journal of Renewable and Sustainable Energy

RESEARCH ARTICLE | DECEMBER 01 2021

An innovative V-shaped piezoelectric energy harvester for wind energy based on the fully fluid–solid-electric coupling

Jianjun Liu; Yujie Chen; Wei Xia; ... et. al

Check for updates

Journal of Renewable and Sustainable Energy 13, 063304 (2021)
https://doi.org/10.1063/5.0059870

View Online
Export Citation
CrossMark

Articles You May Be Interested In

A synergetic hybrid mechanism of piezoelectric and triboelectric for galloping wind energy harvesting

Appl. Phys. Lett. (July 2020)

Enhanced performance of wind energy harvester by aerodynamic treatment of a square prism

Appl. Phys. Lett. (March 2016)

Vortex-Induced vibration of triangular bluff body to piezoelectric energy harvester in laminar flow

AIP Conference Proceedings (November 2022)

Downloaded from http://pubs.aip.org/aip/jrse/article-pdf/doi/10.1063/5.0059870/15719563/063304_1_online.pdf

APL Energy
Bridging basic research and innovative technology that will impact the future
First Articles Coming Soon!
No Article Processing Charges (APCs) through 2023
AIP Publishing

AIP Publishing

Journal of Renewable and Sustainable Energy ARTICLE scitation.org/journal/rse

An innovative V-shaped piezoelectric energy harvester for wind energy based on the fully fluid–solid-electric coupling

Cite as: J. Renewable Sustainable Energy **13**, 063304 (2021); doi: 10.1063/5.0059870
Submitted: 13 June 2021 · Accepted: 7 November 2021 ·
Published Online: 1 December 2021

View Online Export Citation CrossMark

Jianjun Liu, Yujie Chen, Wei Xia, Hong Zuo,[a] and Qun Li[a]

AFFILIATIONS

State Key Laboratory for Strength and Vibration of Mechanical Structures, School of Aerospace Engineering, Xi'an Jiaotong University, Xi'an, China

[a]**Authors to whom correspondence should be addressed:** zuohong@mail.xjtu.edu.cn and qunli@mail.xjtu.edu.cn

ABSTRACT

In order to convert galloping-based vibration energy generated by wind flow into electricity more effectively, an innovative piezoelectric energy harvester (PEH) with V-shaped windward wings is proposed and designed to evaluate its performance in this paper. The V-shaped PEH mainly consists of three components: the main cantilever beam made of an aluminum plate, a piece of macro-fiber piezoelectric composite stuck to the end of the main cantilever beam as the key element of energy harvesting, and a pair of V-shaped windward wings as the structure of the bluff body to produce stronger and more regular vortices in wind flow. Wind tunnel experiments are conducted to evaluate its performance of the output voltages, and the results confirm that the angles of V-shaped wings have dramatically affected the behavior of energy harvesting. A pair of 60° angles was confirmed as the optimal angle for this V-shaped PEH, which can achieve the peak-to-peak value of alternating current voltage ($V_{AC\text{-}PP}$) of more than 100 V when the wind velocity is 10 m/s. Subsequently, the fully fluid–solid-electric coupling for this corresponding two dimensional model is simulated by COMSOL Multiphysics, which expounds the mechanism of swing for this V-shaped PEH under the galloping-based vibration, as well as verifies the rationality of the experimental results.

Published under an exclusive license by AIP Publishing. https://doi.org/10.1063/5.0059870

I. INTRODUCTION

Because of the nonrenewable use of fossil fuels, energy harvesting technologies for green and renewable energy have received a great deal of attention in recent years. Wind energy exists in nature extensively and contains huge kinetic energy. It has attracted a great deal of interest in converting wind energy into electrical power, so that it can be applied in small self-powered electromechanical systems to provide continuous energy.[1–3] Wind energy harvesting based on vortex-induced vibration energy has been considered as a promising solution to power for microelectronic devices due to its inexhaustibility and eco-friendliness. Wind energy can be converted into electricity primarily through the use of piezoelectric energy harvesters (PEH) in the presence of flow-induced vibration.[4–6] Based on the positive piezoelectric effect, the piezoelectric materials, such as lead zirconate titanate (PZT),[7,8] polyvinylidene fluoride (PVDF),[9] and macro-fiber piezoelectric composite (MFC),[10,11] have the capability of converting mechanical energy into electrical energy, and the PEH, as an excellent energy conversion device, has received the most attention because of its compact size, easy production, stable performance, and long service life. In order to expand the PEH technology in the application field of wind energy harvesting, the technology of converting wind energy into electrical power has always been pursued by many researchers.[12,13] There are mainly three common methods of PEH based on wind-induced vibration, including flutter,[14,15] vortex-induced vibration,[16,17] and galloping-based.[18,19] Various types of PEH based on vortex-induced vibration energy from aeroelastic vibration have been summarized and discussed by Abdelkefi *et al.*[20] To harvest wind energy via flutter, Liu *et al.*[15] found that only if the critical wind speed reaches in the wind environment, the harvester system can harvest wind energy stably, and it requires strictly the wind strength in the wind field as well as rigorous control and elaborate design of the energy harvesting, while in the flow field environment, the PEH based on galloping-based vibration or galloping has few requirements for the flow field, and the lateral aeroelastic force formed from vortexes and the pressure difference is mainly required. Therefore, the research about PEH based on galloping vibration has been given wide attention.

The galloping appears because the incoming flow is blocked by the bluff body in the galloping-based, and then the lateral unstable

Downloaded from http://pubs.aip.org/aip/jrse/article-pdf/doi/10.1063/5.0059870/15719563/063304_1_online.pdf

Published under an exclusive license by AIP Publishing

aeroelastic force generated under the influence of the fluid pressure difference drives the PEH vibration. Hence, the design and optimization of the structural shape, size, as well as mass of the bluff body, are quite significant to improve the energy harvesting efficiency of the energy harvester system. Simultaneously, design and installation of the bluff body at the free end of the piezoelectric cantilever beam is a constant scheme adopted by many experts in the research of wind-induced PEH.[2,21,22] The energy harvesting performance of PEH with a D-shaped bluff body was investigated by Sirohi and Mahadik,[23] and the importance of material properties, electrical load, and natural frequency related to the behavior of PEH has also been discussed. Five kinds of bluff bodies with various cross-sectional shapes were compared in the experiment research about wind energy using the PEH by Yang *et al.*,[6] and the results showed that the voltage generated by the PEH with a square prism structure is better than that of a bluff body in other shapes, which also possess outstanding performance over a wide range of wind velocity.

Subsequently, the simulations of fluid–solid interactions related to the flow-induced PEH were carried out by Ding *et al.*[24] in finite element software to investigate the PEH with four cross-sectional shapes of a bluff body. Liu *et al.*[25] had proposed a Y-type three-blade bluff body for wind energy harvesting, and their research indicated that the PEH with a three-blade bluff body could not only generate much higher voltage than that with a square prism bluff body but also require much lower onset wind velocity. Liu *et al.*[26] had proposed a fork-shaped bluff body consisting of two front blades, one middle blade and one rear blade. Simulation results of fluid–solid interactions showed that the average fluid lift on the fork-shaped structure was greater than those of other cases, and subsequent experimental results also verified the above conclusions. That is, the shape and structure of the bluff body have an obvious influence on the performance of PEH in the field of galloping-based energy harvesting. As a result, a well-designed and optimized bluff body can significantly improve PEH's performance and efficiency in the wind field environment.

In this paper, an innovative V-shaped PEH is proposed and designed to convert more galloping-based vibration energy generated by wind flow into electricity. It consists of a piezoelectric cantilever beam with macro-fiber composite (MFC) and a pair of V-shaped windward wings with various angles. Wind tunnel testing is used to investigate the performance of the V-shaped PEH, and the mechanism of energy harvesting employed by this V-shaped PEH is expound using a simulation of fully fluid–solid-electric coupling. The following is how this paper is structured. Section II elaborated on the concept and design for V-shaped PEH using MFC. In Sec. III, wind tunnel experiments were performed; in Sec. IV, the simulation of fully fluid–solid-electric coupling was investigated; and in Sec. V, a brief conclusion was presented.

II. THE IDEA AND DESIGN FOR V-SHAPED PEH USING THE MFC

In this paper, inspired by the symmetrical leaves swaying in the wind, a novel V-shaped PEH is proposed and designed to harvest wind energy and convert it into electric power using piezoelectric materials. Among various piezoelectric materials that have been used for energy harvesting, the PZT ceramics[27,28] are too brittle and easily broken to apply to large continuous deformations, and the piezoelectric coefficient of PVDF[29–31] is too low for the energy harvester. MFC,[32] invented by NASA Langley Research Center in 1999, is widely utilized in the fields of low-profile actuator, sensor, and energy harvester for the advantages of high performance, flexibility, and reliability in a cost-competitive device. The MFC is constructed with piezoelectric fibers and interdigital electrodes embedded in a polymer matrix such as epoxy resin and polyimide, as shown in Fig. 1(a). It exhibits excellent flexibility in large deformations and reliability in electronic devices. Therefore, these excellent properties make it an energy harvester transferring wind energy into electrical energy.[33,34] In this paper, the MFC-P2-2814, as shown in Fig. 1(b), is selected as the main material for this designed V-shaped PEH to explore the behavior of energy harvesting.

The proposed V-shaped PEH mainly consists of three components: a main cantilever beam made from an aluminum plate, a piece of MFC stuck to the end of the main cantilever beam as the key element of energy harvesting, and a pair of V-shaped windward wings as the structure of the bluff body to produce stronger and more regular vortices in wind flow. The schematic diagram and experimental design of the proposed V-shaped PEH are shown in Fig. 2.

The process of energy harvesting from the wind flow using the V-shaped PEH in the wind field is as shown in Fig. 3. The V-shaped PEH is installed upstream in the wind flow field first, as shown in Fig. 3(a), and the opening direction of the V-shaped windward wings faces the incoming wind flow. The wind flow is blocked by the windward wing when it flows through this PEH, and then the asymmetric vortex streets are formed on each side of the V-shaped windward wing. As the wind moves forward, the asymmetrical vortex street will form on a regular basis, and different wind pressures ΔP will be generated on each side of the windward wing, as shown in Figs. 3(b) and 3(c). It is just the transverse lift force from the galloping-based of difference in pressure that drives the windward wings and the main cantilever beam to swing left and right. The main cantilever beam will be bent and deformed periodically, and the strain generated by the bending deformation will be transferred to the piezoelectric materials. Based on the piezoelectric effect, piezoelectric materials generate positive and negative charges on their surface. Then, the charge is collected to form an electric current through an external circuit, and the wind energy will be converted into electrical power by the V-shaped PEH finally.

The novel V-shaped PEH proposed in this paper swings upon the galloping-based vibration, which mainly depends on the influence of angles between the windward wings, and the cantilever beam is

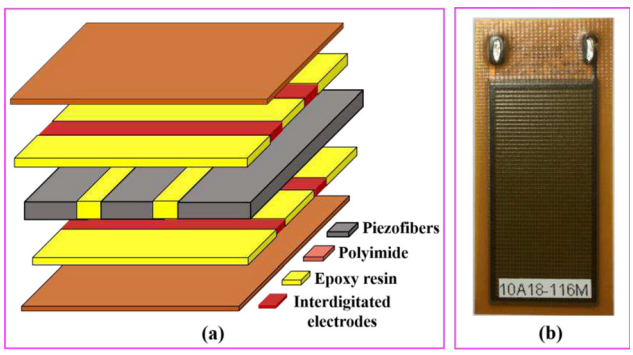

FIG. 1. The piezoelectric materials MFC: (a) the cross-sectional layout of the MFC; (b) MFC-P2-2814 used in this experiment (Smart Material Corp).

Downloaded from http://pubs.aip.org/aip/jrse/article-pdf/doi/10.1063/5.0059870/15719563/063304_1_online.pdf

Published under an exclusive license by AIP Publishing

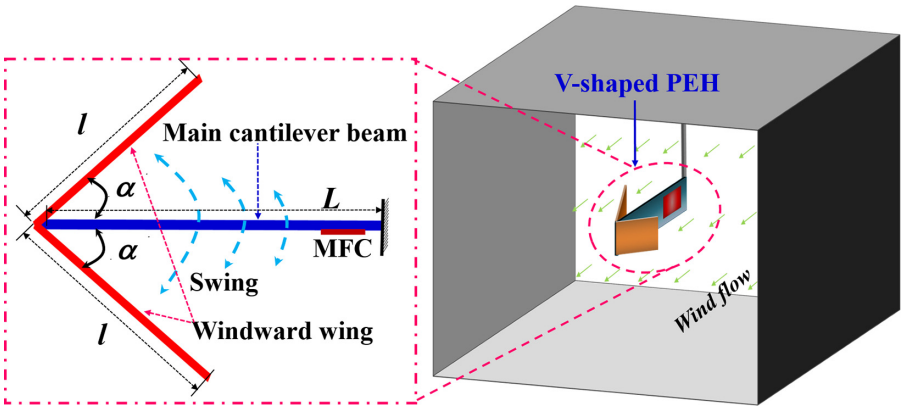

FIG. 2. Schematic diagram of V-shaped PEH in wind flow field.

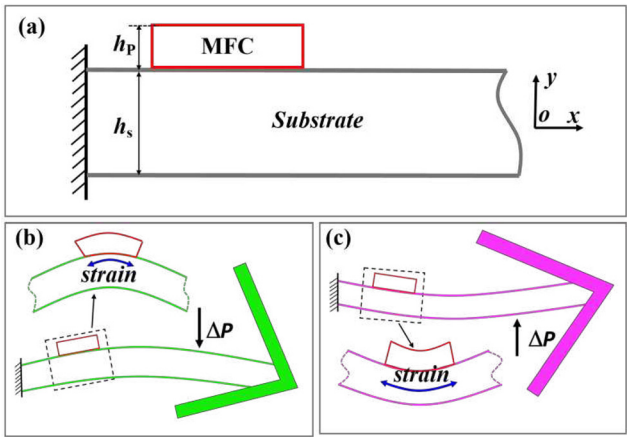

FIG. 3. Schematic diagram of energy harvesting for V-shaped PEH under wind load pressure: (a) equilibrium position, (b) convex-shape swing, and (c) concave-shape swing.

concerned. Different angles of windward wings have different effects on blocking wind flow, and the generated pressure differential varies. That is, swing features of windward wings with different angles in wind flow differ. The behavior of wind energy harvesting using the PEH with windward wings in different angles is investigated, including the influence of wind velocity on it. The aim of this paper is to find the optimal angle of windward wings so as to improve the efficiency of energy harvesting for V-shaped PEH in the wind flow.

The coupling of this V-shaped PEH harvests the galloping-based vibration energy from wind flow into electricity. This system consists of the fluid–solid coupling of the vortex shedder and wind flow, and the fluid–structure coupling and electro-mechanical coupling of the piezoelectric cantilever beam and wind flow.

III. EXPERIMENT IN WIND TUNNEL

A. Experimental apparatus of PEH in wind tunnel

To measure the energy harvesting behavior of the novel V-shaped PEH under different wind velocities, a series of experiments about the influence of various windward wing angles on the energy

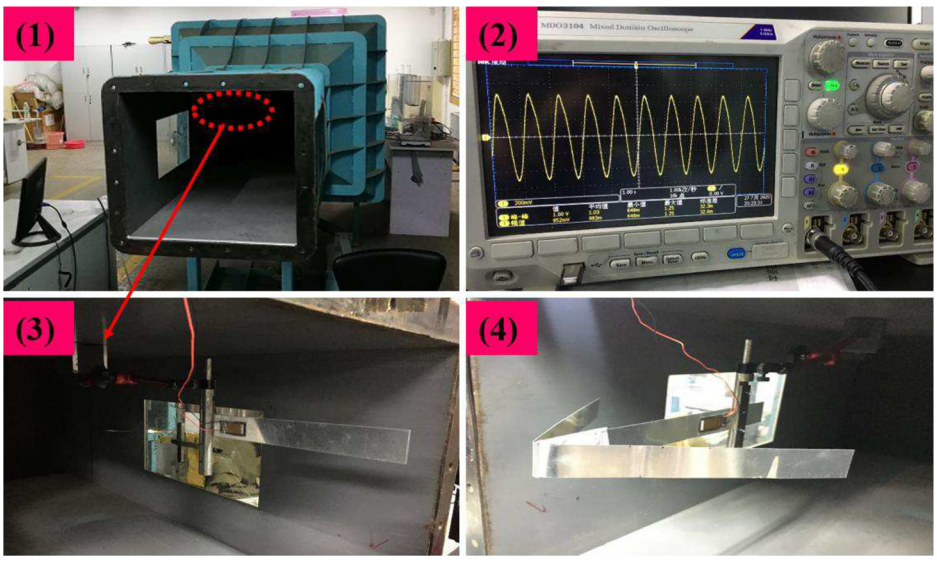

FIG. 4. The V-shaped PEH system in wind tunnel laboratory apparatus: (1) the wind tunnel, (2) oscilloscope (DPO-2012B, resistance: 1 MΩ), (3) the fixed V-shaped PEH without the structure of V-shaped wing in the wind tunnel, and (4) the V-shaped PEH with V-shaped wings in $\alpha = 60°$ angle fixed in wind tunnel.

Downloaded from http://pubs.aip.org/aip/jrse/article-pdf/doi/10.1063/5.0059870/15719563/063304_1_online.pdf

Published under an exclusive license by AIP Publishing

harvesting are performed in an open circuit wind tunnel (cross section: 500 × 500 mm^2; wind speed: ≤ 20 m/s) in the Aerodynamics Laboratory, School of Aerospace, Xi'an Jiaotong University, China. The wind velocity in the wind tunnel is collected by a pitot tube and calibrated by an anemometer. The laboratory apparatus for wind energy harvesting is shown in Fig. 4. In the experiments, the main cantilever beam and the windward wings are made of aluminum plates with 30 mm width and 0.8 mm thickness, and their length is 300 and 200 mm, respectively. The structure of windward wings is installed on the free end of the main cantilever beam, and a piece of M2814-P2, as shown in Fig. 1(b), is bonded on the other end of the main cantilever beam. The V-shaped PEH is installed on the inner upper surface of the open wind tunnel using a magnetic base. An oscilloscope (TektronixDPO-2012B) with a 1 MΩ internal load resistance R_0 is used to measure the voltage value that was obtained through experimental exploration in this article. The MFC is connected to a digital storage oscilloscope to form a circuit loop, as shown in Fig. 5. The MFC will generate a current $\boldsymbol{i}$ and circulate in the circuit loop while the harvester is operational. The oscilloscope's load resistance R_0 (1 MΩ) is substantially higher than the MFC's load resistance R_{MFC} (10–50 KΩ). The voltage drop across the R_0 is substantially higher than that across MFC based on the theory of load resistance divided voltage, and the voltage drop from the MFC is small and almost negligible, and the voltage across the load resistor R_0 is displayed by an oscilloscope; therefore, the electrical measurements by the oscilloscope can be regarded as precise.

In the following analysis of the results, the instantaneous alternating voltage directly displayed on the oscilloscope and its peak-to-peak voltage value ($V_{AC\text{-}PP}$) will be collected to explore the characteristics of the behavior of V-shaped PEH in this paper. The $V_{AC\text{-}PP}$, which represents the average value of the difference between the maximum and minimum value of instantaneous alternating voltage in N cycles, can be written as

$$V_{AC-PP} = \frac{1}{N}\sum_{i=1}^{N} |V_i^{max} - V_i^{min}|. \quad (1)$$

B. Experimental results

The results of output voltage by the PEH system without V-shaped wings (only with the piezoelectric cantilever beam) and by the PEH system with V-shaped wings designed in this paper are compared. Figure 6(a) shows the transient alternating voltage generated by PEH without a V-shaped wing and with windward wings at an a = 60° angle under 5 m/s wind velocity, and Fig. 6(b) shows the transient alternating voltage generated by PEH under 10 m/s wind velocity. It can be seen from the results that the transient voltage generated from PEH without a V-shaped wing is less than ±2 V whether at a wind velocity of 5 or 10 m/s. While the voltage generated by PEH with V-shaped wings is up to ±15 V at a wind velocity of 5 m/s, and when the wind velocity increases to 10 m/s the voltage can range from −52 to +43 V. Obviously, the PEH with V-shaped wings has better performance than the PEH without V-shaped wings. The swinging performance of the V-shaped windward wing structure has been improved greatly in the wind environment, and the voltage output via the PEH system increases remarkably.

The output of transient voltage response is shown in Fig. 7 for V-shaped PEH with various angles of α = 15°, 30°, 45°, 60°, 75°, 90°, 120°, 135°, and 150° under wind velocity of 10 m/s, and the results of

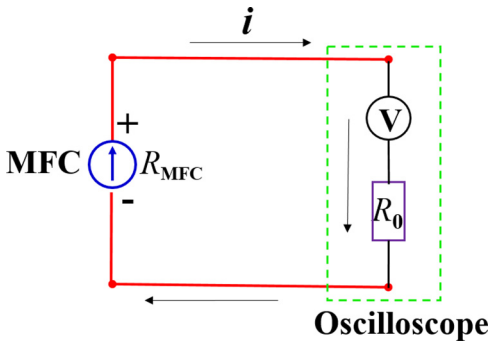

FIG. 5. Diagram of a circuit loop made up of an oscilloscope and an MFC.

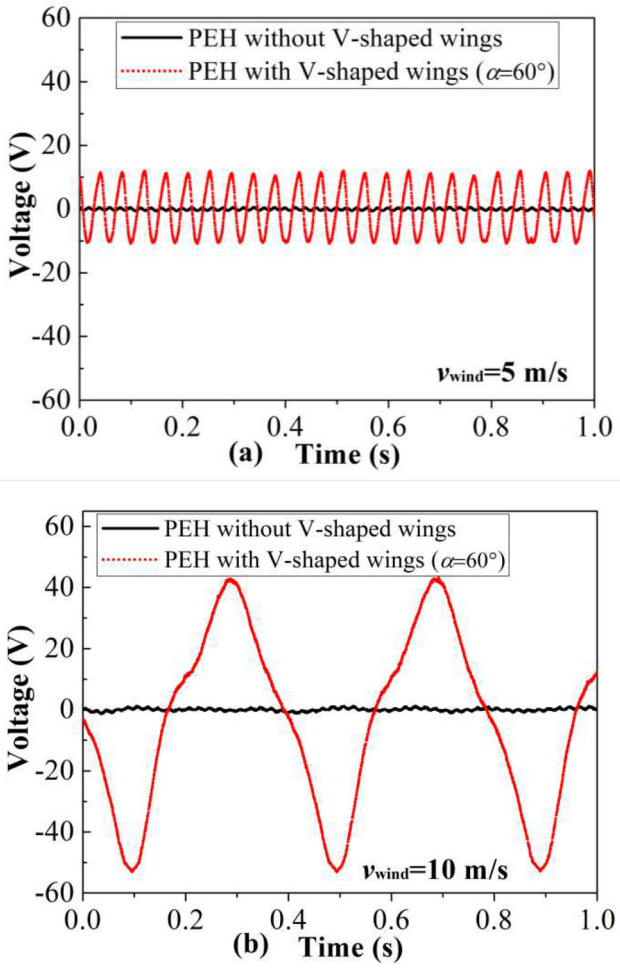

FIG. 6. The experimental result of output voltage compared with PEH without V-shaped wing and V-shaped wings in the angles of 60° at a wind velocity of (a) 5 and (b) 10 m/s.

Downloaded from http://pubs.aip.org/aip/jrse/article-pdf/doi/10.1063/5.0059870/15719563/063304_1_online.pdf

Published under an exclusive license by AIP Publishing

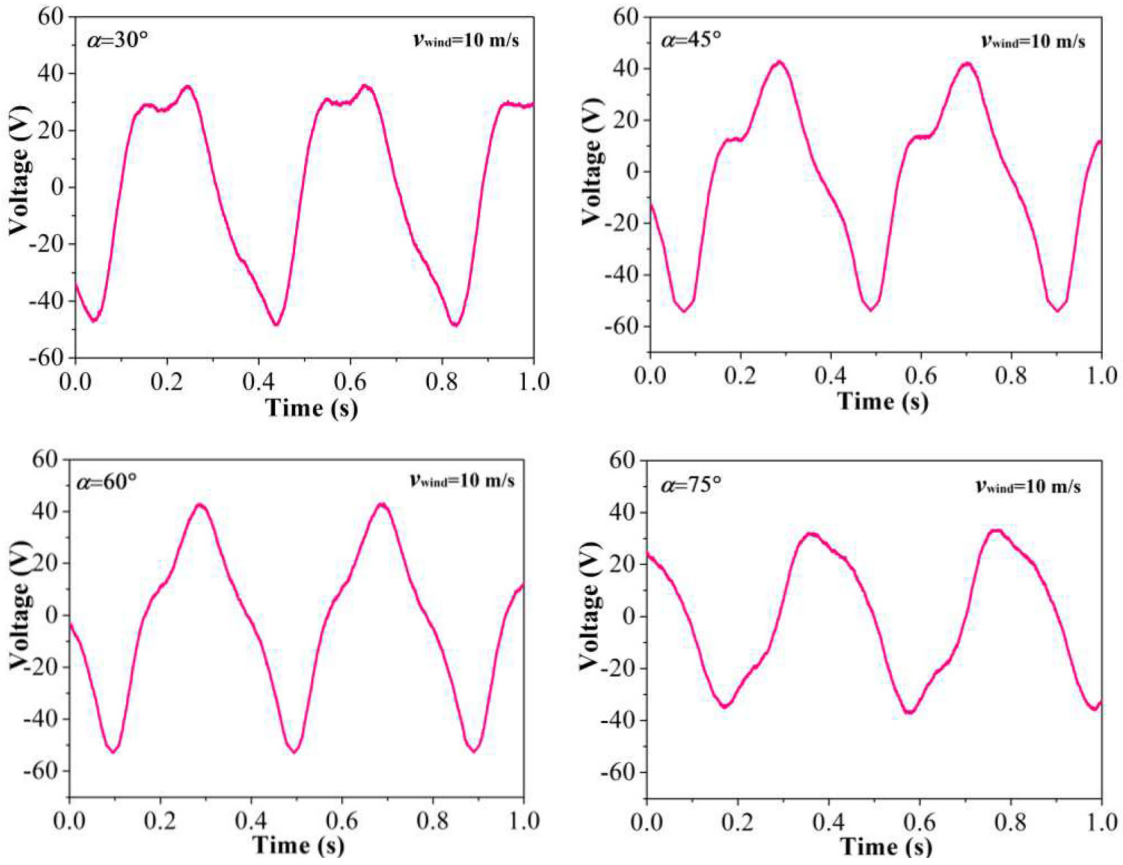

FIG. 7. The transient voltage output by PEH system with windward wings in various angles under the wind flow environment.

$V_{AC\text{-}PP}$ output generated by the harvester with various angles of $\alpha = 15°$, 90°, 120°, 135°, and 150°are listed in Table I in detail. From Table I, we found that the $V_{AC\text{-}PP}$ output generated by the harvester with angles of $\alpha = 15°$, 90°, 120°, 135°, and 150° is not more than 2 V. The transient voltage generated by the V-shaped PEH with an angle of $\alpha = 60°$, on the other hand, is greater than 50 V, which is nearly 50 times greater than the transient voltage generated by the V-shaped PEH with angles of $\alpha = 15°$, 90°, 120°, 135°, and 150°. In consequence, as to the output voltage, the largest voltage is generated from the V-shaped PEH with angles of $\alpha = 60°$ and then angles of $\alpha = 45°$, followed by angles of $\alpha = 30°$ and 75°.

The $V_{AC\text{-}PP}$ generated from V-shaped PEH with a series of different angles is collected by the oscilloscope in the wind tunnel at a velocity of 3–10 m/s, as shown in Fig. 8. The experimental results show that the $V_{AC\text{-}PP}$ increases with the growth of wind velocity. Specially, the output $V_{AC\text{-}PP}$ grows rapidly when the wind velocity reaches 5 m/s, and then the output $V_{AC\text{-}PP}$ grows slowly along with the wind velocity increasing. It is always the V-shaped PEH with angles of $\alpha = 60°$ that outputs the highest $V_{AC\text{-}PP}$ in the wind flow with different velocities. When the wind velocity is 10 m/s, the $V_{AC\text{-}PP}$ is near 100 V, and then it decreases rapidly with the increase in windward angles. While the angle of windward is more than $\alpha = 90°$, the $V_{AC\text{-}PP}$ generated from V-shaped PEH decreases to 3.5 V. The experiment results of $V_{AC\text{-}PP}$ output by V-shaped PEH with different angles under different wind velocities are listed in Table II in detail. The experiment phenomenon and its cause will be discussed in greater detail in the following simulation section.

IV. SIMULATION OF FULLY FLUID-SOLID-ELECTRIC COUPLING FOR V-SHAPED PEH

A. Establishment of the model of fully fluid-solid-electric coupling

The numerical model of V-shaped PEH has been established to investigate the influence of windward-wing on the performance of energy harvesting in a wind flow field based on the computational

TABLE I. The results of voltage output generated by the harvester with various angles of $\alpha = 15°$, 90°, 120°, 135°, and 150°.

α (°)	15	90	120	135	150
Voltage (V)	−0.5–0.5	−0.75–0.25	−0.5–1.0	−0.5–0.5	−0.25–0.75

Downloaded from http://pubs.aip.org/aip/jrse/article-pdf/doi/10.1063/5.0059870/15719563/063304_1_online.pdf

Published under an exclusive license by AIP Publishing

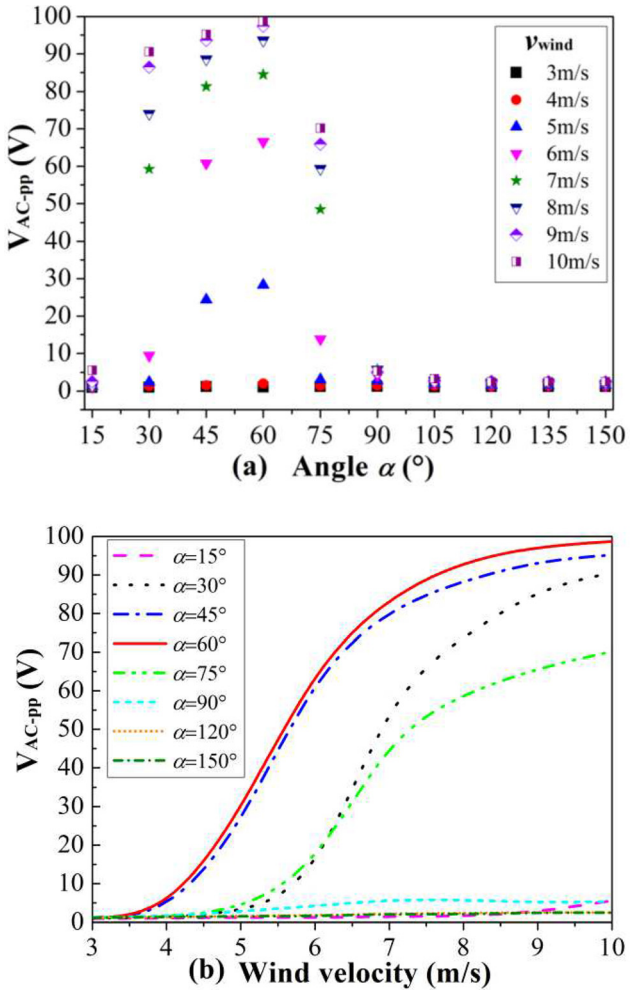

FIG. 8. The influence of (a) windward wing angles and (b) wind velocity on the V_{AC-PP} output generated by V-shaped PEH.

fluid dynamics method. The large eddy simulation (LES)-Smagorinsky module of COMSOL Multiphysics software is utilized for the simulation of fully fluid–solid-electrical coupling. The cross-sectional size of the wind flow field is a two-dimensional rectangle of 800 × 1500 mm^2, as shown in Fig. 9. The entire surface area is the movement area for wind flow, and air with a viscosity coefficient of 1.85×10^{-5} Pa s is chosen as the wind field for simulation calculation in the wind field. The wind flow enters from the left side of the wind field and exits from the right, with the upper and lower sides of the flow field are the non-slip boundaries of the flow field. The V-shaped PEH is positioned 300 mm to the left of the wind tunnel inlet, with the opening direction facing the wind tunnel inlet. Obviously, the V-shaped PEH is positioned in the center of the flow field in the y direction for the computation to be exact and reasonable. The lengths of the main cantilever and the windward wing are 300 and 200 mm, respectively, and the thickness (or height) is all 10 mm. The MFC is pasted on the upper surface 20 mm from the fixed end of the main cantilever in the x direction, and the dimensions of it are a rectangle of 60 × 6 mm^2.

TABLE II. The experiment results of V_{AC-PP} (V) output generated by the V-shaped PEH with various angles of windward wings in different wind velocities.

α (°) \ v_{wind} (m/s)	3	4	5	6	7	8	9	10
15	0.96	0.97	1.17	1.28	1.45	1.48	2.54	5.60
30	0.98	1.35	2.39	9.46	59.26	74.08	86.46	90.56
45	1.21	1.52	24.35	60.80	81.36	88.58	93.60	95.20
60	1.08	2.03	28.30	66.54	84.52	93.62	97.40	96.68
75	1.16	1.42	3.10	13.82	48.45	59.34	65.92	70.20
90	1.23	1.49	2.83	4.16	5.80	5.81	5.85	6.01
105	1.08	1.39	1.93	2.18	2.41	2.66	2.81	3.26
120	1.19	1.22	1.62	1.76	2.25	2.28	2.47	2.63
135	1.19	1.30	1.50	1.88	1.96	2.33	2.43	2.53
150	1.16	1.33	1.56	1.56	2.10	2.13	2.46	2.48
165	1.09	1.19	1.39	1.68	2.22	2.27	2.32	2.58

Subsequently, the initial wind speed is v_{wind} and a step function is superimposed on the wind speed to ensure that the wind speed is a continuous process from 0 to v_{wind}, thereby ensuring the convergence of the simulation calculation. The 11 kinds of angles α range from 15° to 165° with an interval of 15°, and the wind velocity v_{wind} range of 3–10 m/s is selected for simulation calculation of the V-shaped PEH. The computational mesh configuration of the V-shaped is guided by the physical field, as shown in Fig. 10. Finally, the time step is set to 0.01 s, and the calculation time is 1 s. The fluid–solid interaction calculation is carried out for the transient issue in the finite element software. The detailed material parameters required for simulation calculation are shown in Table III.

B. Analysis for simulation results of fluid–solid-electric fully coupling model

Based on the analysis of the vortex, the feature of the V-shaped PEH system with an angles of α = 60° swinging in the wind flow is observed and explored by the swinging displacement curve, as shown in Fig. 11. It is found that the displacement for PEH with V-shaped is much larger than that without V-shaped. After a brief period of transient response process, the energy harvester's vibration settles into

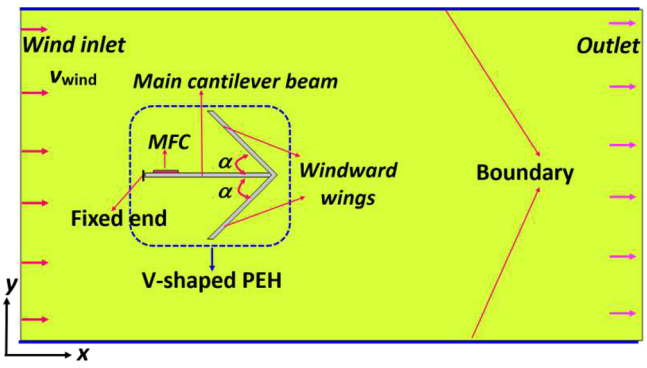

FIG. 9. Two-dimensional numerical model of windward-swing PEH in the wind flow field.

Downloaded from http://pubs.aip.org/aip/jrse/article-pdf/doi/10.1063/5.0059870/15719563/063304_1_online.pdf

Published under an exclusive license by AIP Publishing

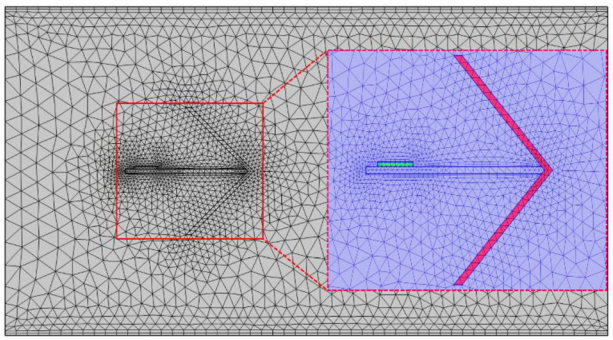

FIG. 10. The mesh of computational model with V-shaped structure.

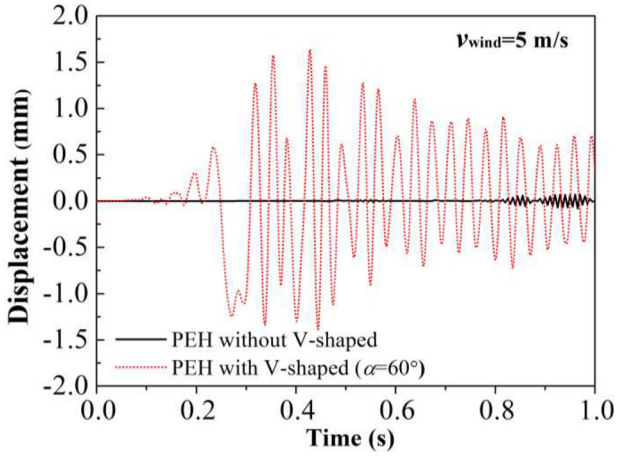

FIG. 11. The displacement (Y-direction) of PEH system with windward wings in angle $\alpha = 60°$ at wind velocity 5 m/s.

stable limit cycle oscillation. In the following stage, it swings steadily. The displacement curve is like sinusoidal variation, and the lift force to drive the windward wings is also sinusoidal variation with time.

It is intuitively speculated that the angles of V-shaped PEH and wind velocity will directly affect the transverse wind lift force acting on the windward wings, and therefore, a series of simulations of full fluid–structure-electric coupling for V-shaped PEH with various angles at different wind intensities have been performed. The simulation results of the vorticity magnitude field (1/s), wind load pressure (Pa), and wind velocity field (m/s) for this PEH with angles of $\alpha = 45°$ at wind velocity 5 m/s are presented in Fig. 12.

When wind flows through the V-shaped PEH, the track of the wind forward alters because of the blocking effect of the opening windward wings, and the wind speed is significantly reduced on the inner part of the windward wing as shown in Figs. 12(c1)–12(c4). At this moment, wind flows pass through the inner surface of windward wings to the outside and then forms positive- and negative-vorticity zones that alternately distribute at the upper end of the wings. Subsequently, the vorticity on the outside surface continues to increase and periodically generates and sheds alternately, as shown in Figs. 12(a1)–12(a4). The change in vortex positions leads to constant variations in the pressure difference between the interior and outside surfaces of the wings, as shown in Figs. 12(b1)–12(b4). The V-shaped PEH swings up and down on a regular basis as the difference in wind-load pressure moves, generating transverse lift that forces the windward wings wave up and down. Figure 12 depicts four different swing states of V-shaped PEH in a vibration cycle if T is the motion period. When t = 0 and t = 0.5 T, the equilibrium position of the main piezoelectric cantilever beam is shown in Figs. 12(b1) and 12(b3); at this time, the sine-like oscillatory transverse aerodynamic force was zero. The maximum amplitude displacement up and down of the main piezoelectric cantilever beam occurs when t = 0.25 and t = 0.75 T, as shown in Figs. 12(b1) and 12(b3).

TABLE III. Material properties available in fully fluid–solid-electric coupling.[35]

Wind flow (air)	ρ (kg/cm^3)	1.205
(20 °C, 1 atm)	Dynamic viscosity (Pa/s)	1.8×10^{-5}
Aluminum	ρ (kg/cm^3)	2700
	Young's modulus, E (GPa)	70
	Possion's ration ν	0.33
MFC-P2-2814	Young's modulus, E (GPa)	30.336
	Possion's ration ν	0.31
	Piezoelectric constant d_{31} (pc/N)	−174
	Piezoelectric constant d_{33} (pc/N)	410
	Dielectric permittivity ε_{33}	1700

The change in wind velocity in the wind field is displayed in Figs. 12(c1)–12(c4). The given original velocity of incoming wind is 5 m/s, and wind velocity in the near and rear areas of the PEH alters obviously when the vortex exists. The wind speed draws near zero inside the V-shaped PEH due to the stagnation region[36] induced by the blocking of wings, whereas the wind speed in the rear of the PEH reaches nearly twice the original velocity, near 10 m/s. The primary cause of the varying wind velocity distribution in the wind field is that the windward wings block the forward flow tracks of wind, resulting in eddy current and wind-load pressure. The wind velocity distribution in the wind field is then influenced.

In order to explore the influence of windward wing angles on the vortexes, the simulation results of V-shaped PEH with angles of $\alpha = 15°, 60°, 90°, 135°, 165°$ at wind velocity 5 m/s are selected to illustrate in Fig. 13. When the angle is small, as shown in Figs. 13(a1)–13(a4), the effective area of blocking wind by windward wings is small, which results in a very small change in vortex strength; therefore, the corresponding swing amplitude of windward wings is not very large. When the effective area of blocking wind by windward wings increases with the increase in angles, the induced vortex strengthens correspondingly, and then the swing amplitude with angles $\alpha = 60°$ reaches its maximum when compared to angles $\alpha = 30°, 45°$, and 75°. When the angle is 90°, the positive and negative vortexes that are generated and fallen off alternately are nearly symmetric, resulting in a small vortex strength differential and swing amplitude. When the angles are greater than 90°, the blocking effect of the windward wings is significantly reduced and the vortexes still generate and fall off alternately, but the intensity of the vortexes decreases.

Downloaded from http://pubs.aip.org/aip/jrse/article-pdf/doi/10.1063/5.0059870/15719563/063304_1_online.pdf

Published under an exclusive license by AIP Publishing

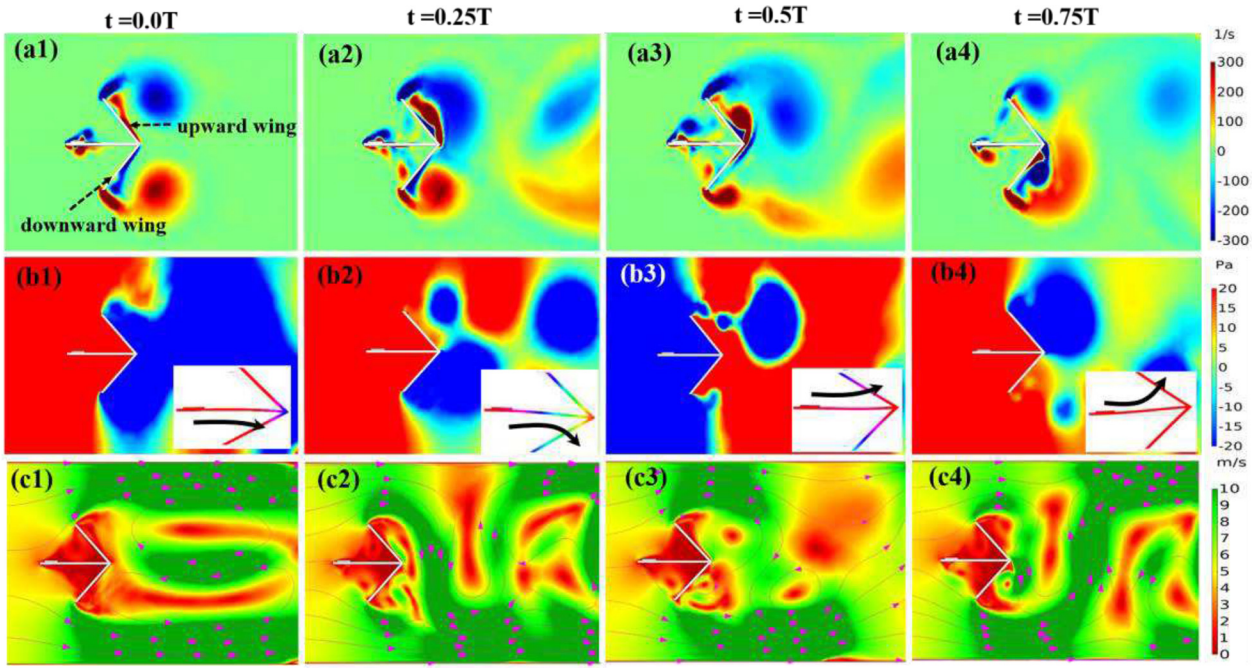

FIG. 12. The simulation results of fully fluid–structure-electric coupling (a) vorticity magnitude distributions, (b) pressure distributions (the swing deformation of V-shaped PEH is shown in the lower right corner), and (c) wind velocity field for this windward-swing PEH with the windward wings in $\alpha = 45^\circ$ at wind velocity 5 m/s.

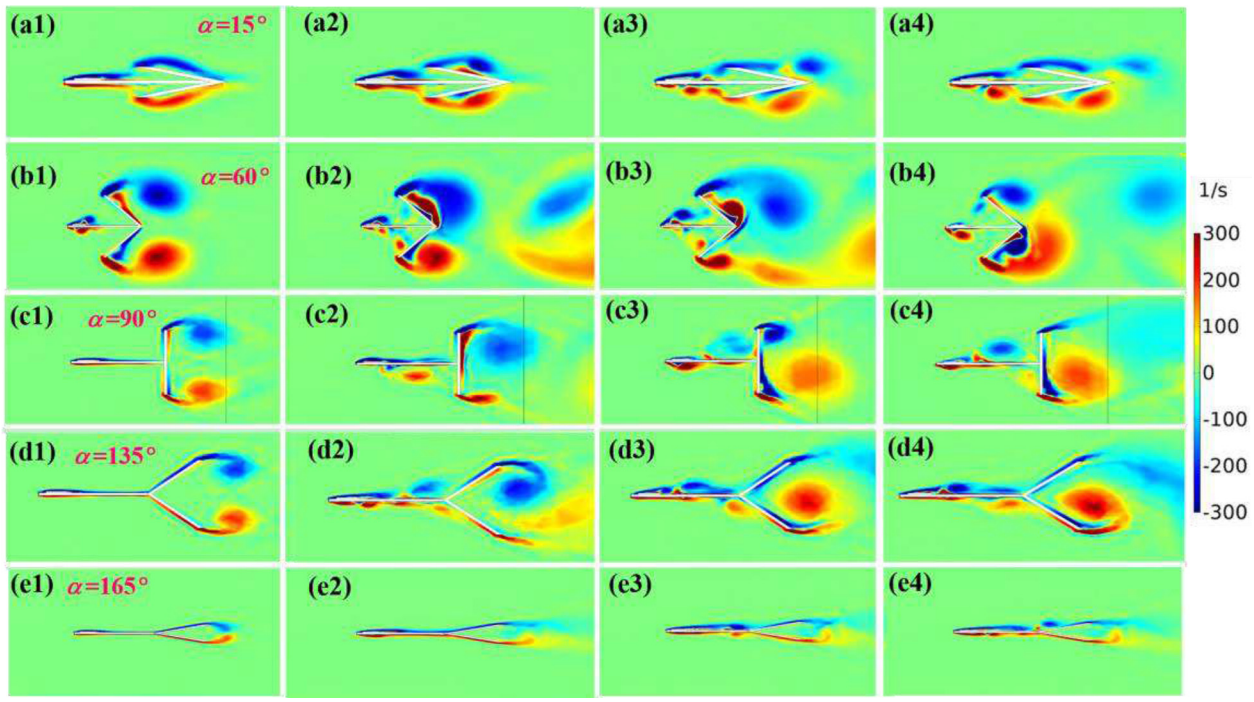

FIG. 13. The vorticity magnitude distributions with various windward wing angles at a variation period at wind velocity 5 m/s. (a)–(e) The angles $\alpha = 15^\circ$, 60°, 90°, 135°, and 165°, respectively.

Downloaded from http://pubs.aip.org/aip/jrse/article-pdf/doi/10.1063/5.0059870/15719563/063304_1_online.pdf

Published under an exclusive license by AIP Publishing

In order to investigate the influence of various angles and wind speed on the performance of V-shaped PEH, the voltage generated via the V-shaped PEH with varied angles needs to be analyzed further. The virtual circuit with an external resistance value of 1 MΩ was selected to collect the output voltage.

The simulation result of transient output voltage generated from V-shaped PEH with angles of $\alpha = 30°$, 45°, 60°, and 150° under the wind velocity of 5 m/s and 10 m/s is as shown in Fig. 14. When the wind velocity is 5 m/s, the V-shaped PEH with an angle of $\alpha = 60°$ generates a steady alternating voltage of roughly ±10 V. However, the output voltage is only in the range of −0.5 V∼ +1 V when this PEH is with an angle of $\alpha = 30°$, and when the angle is $\alpha = 150°$, the output voltage is only −0.4 V ∼ +0.2 V. The voltage output by the V-shaped PEH with angles of $\alpha = 30°$ and 150° is quite lower than that of the V-shaped PEH with angles of $\alpha = 45°$ and 60°, and the output voltage signals are unstable. The reason is that the V-shaped PEH with angles of $\alpha = 30°$ and 150° can only vibrate slightly or swing gently in the wind field, which makes it difficult to harvest more electricity due to the swing from side to side insufficiently. Therefore, the performance of the V-shaped PEH with an angles of $\alpha = 30°$ and 150° is not accepted. When the wind velocity is 10 m/s, a V-shaped PEH with an angle of $\alpha = 30°$ can produce about ±40 V voltage, a rapid increase, although it is still smaller than that of both V-shaped PEH with angles of $\alpha = 60°$ and 45°, which can output about 58 and 50 V, respectively. It suggests that the wind velocity has significant influence on the performance of the V-shaped PEH with an angle of $\alpha = 30°$. The voltage output by it with an angle of $\alpha = 150°$ is still below ±0.5 V, which is not affected by the increase in of wind velocity.

The simulation results of the $V_{AC\text{-}PP}$ generated by V-shaped with various angles under the wind velocity range from 3 to 10 m/s are presented in Fig. 15. It is obvious that the $V_{AC\text{-}PP}$ of the V-shaped PEH with varied angles increases as the wind velocity increases. The $V_{AC\text{-}PP}$ increases rapidly when the wind velocity exceeds 5 m/s. The output $V_{AC\text{-}PP}$ then grows slowly as the wind velocity increases. When the wind velocity is 10 m/s, the $V_{AC\text{-}PP}$ is more than 100 V, and then it decreases rapidly as the windward wings angles increase. While the angle of windward wings exceeds 90°, the $V_{AC\text{-}PP}$ generated from PEH decreases to below 2 V. Windward wings with varying angles have

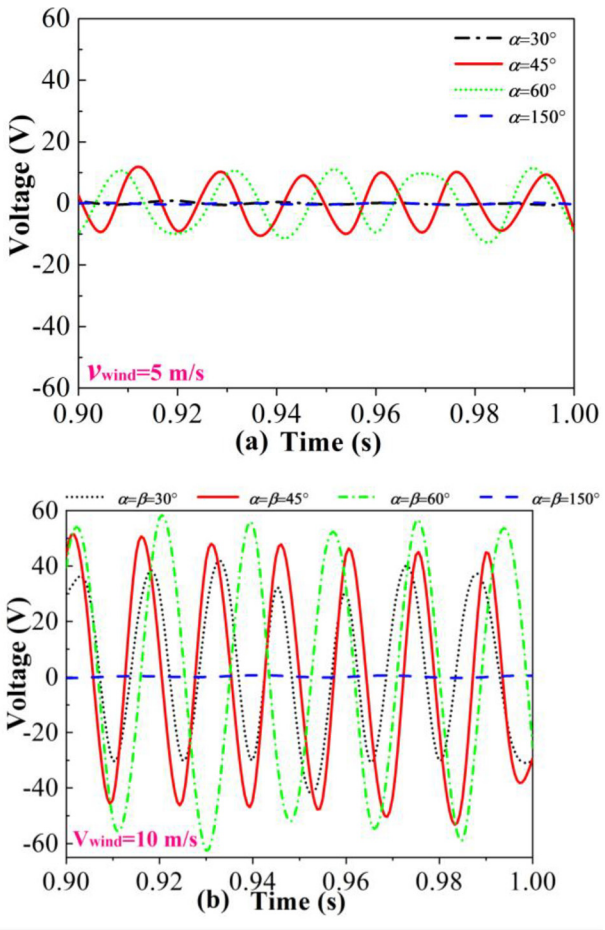

FIG. 14. The transient voltage output by the simulation of fully fluid–structure-electric coupling in angles of 30°, 45°, 60°, and 150° under wind velocity: (a) 5 and (b) 10 m/s.

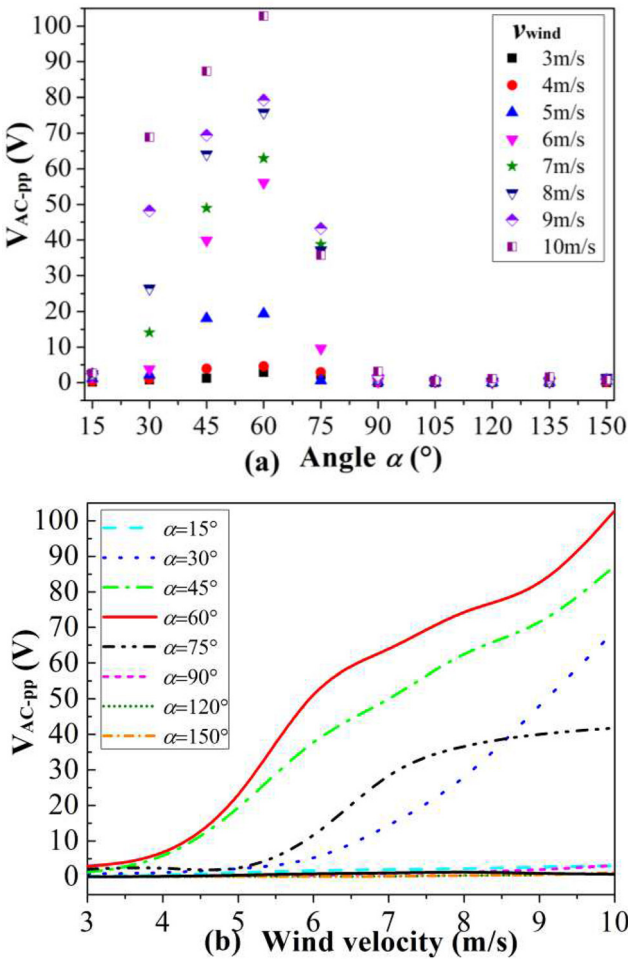

FIG. 15. The simulation results of the $V_{AC\text{-}PP}$ generated by V-shaped with (a) various angles and (b) the wind velocity range from 3 to 10 m/s.

Downloaded from http://pubs.aip.org/aip/jrse/article-pdf/doi/10.1063/5.0059870/15719563/063304_1_online.pdf

Published under an exclusive license by AIP Publishing

variable blocking effects, and produced vortexes and wind-load pressure are different on the inside and outside surfaces of windward wings. Because the transverse lift generated to push the windward wings wave varies with different angles, the $V_{AC\text{-}PP}$ of the PEH with windward wings varies as well. Among the various angles of windward wings, the V-shaped PEH with the windward wings at an angle of $\alpha = 60^\circ$ has the best swing performance, and consequently the highest voltage generated. The simulated results and trend are very similar to the experimental results.

C. The validation of the numerical results

For the V-shaped PEH device, the influence of the wind velocity, vorticity magnitude field, pressure field, and effective vortex shedding frequency in the flow field will be further analyzed in this section in order to verify the energy harvesting characteristics for the designed V-shaped PEH device. As shown in Fig. 16, when the angle of the V-shaped PEH is the same, the wind speed intensity on the top and lower sides of the V-shaped wing in the wind field gradually increases as the wind speed intensity at the air inlet increases, according to the research. The pressure difference generated on both sides of the V-shaped wing will grow as the strength of the vortex field formed at the tail ends of the V-shaped wings grows. This shows that as the wind speed increases, the wind-induced pressure on the V-shaped PEH will increase.

As shown in Fig. 17, when the same initial wind speed flows through the V-shaped PEH in the flow field, the wind speed strength on the upper and lower sides of the V-shaped wing will be significantly different due to the angle difference. The wind speed is stronger when the angle is 60°, and it is smaller when the angle is 150°. The intensity of the vortex field generated at the tail ends of the two wings is also the strongest when the wind speed in the flow field is high, and the pressure difference formed on the inner and outer sides of the two wings is also the highest. As a result, the V-shaped PEH with an angle of 60° in the flow field has the highest wind pressure and vibration amplitude, as well as the highest output voltage. Through numerical values, this verifies the reasonableness of the experimental results.

Beam-type piezoelectric harvesters rely on resonance; not enough power is harvested if the excitation frequency is not equal to the resonant frequency of the beam. The relationship between the frequency of the effective vortex shedding generated by the wind in the flow field passing through the V-shaped PEH with various angles and the natural frequency of the V-shaped PEH system is investigated further in this work. The relationship between the effective vortex shedding frequency of V-shaped PEH with varied angles in the flow field and wind speed intensity is as shown in Fig. 18. The effective vortex shedding frequency in this article refers to the frequency of the vortex after it has fallen off in the front and rear regions of the two V-shaped wings. After analyzing the information, it was discovered that the effective vortex shedding frequency in the flow field is positively connected to the wind speed intensity range, i.e., it increases as wind speed increases. The effective vortex shedding frequency of V-shaped PEH with angles of 30°, 45°, and 60° increases dramatically as wind speed

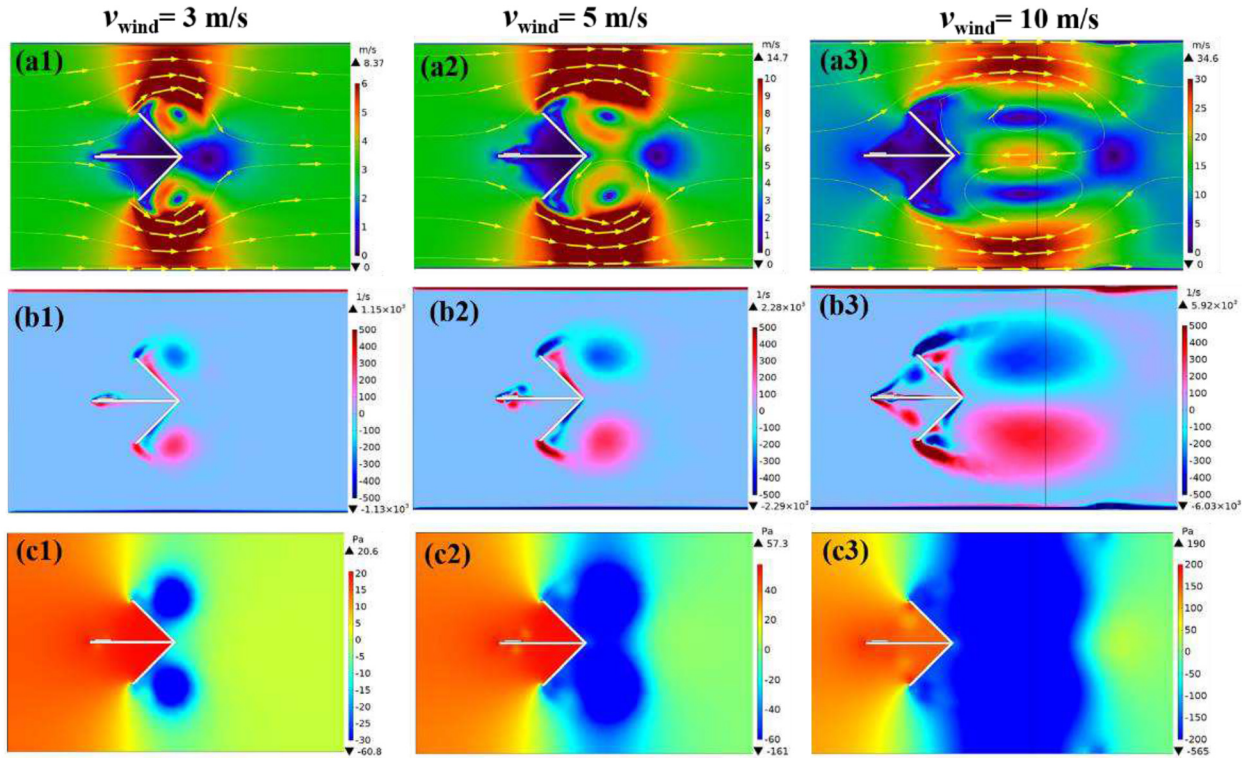

FIG. 16. The simulation results of fully fluid–structure-electric coupling (a) wind velocity field, (b) vorticity magnitude distributions, and (c) pressure distributions for V-shaped PEH with an angle of 45° at various wind velocities.

Downloaded from http://pubs.aip.org/aip/jrse/article-pdf/doi/10.1063/5.0059870/15719563/063304_1_online.pdf

Published under an exclusive license by AIP Publishing

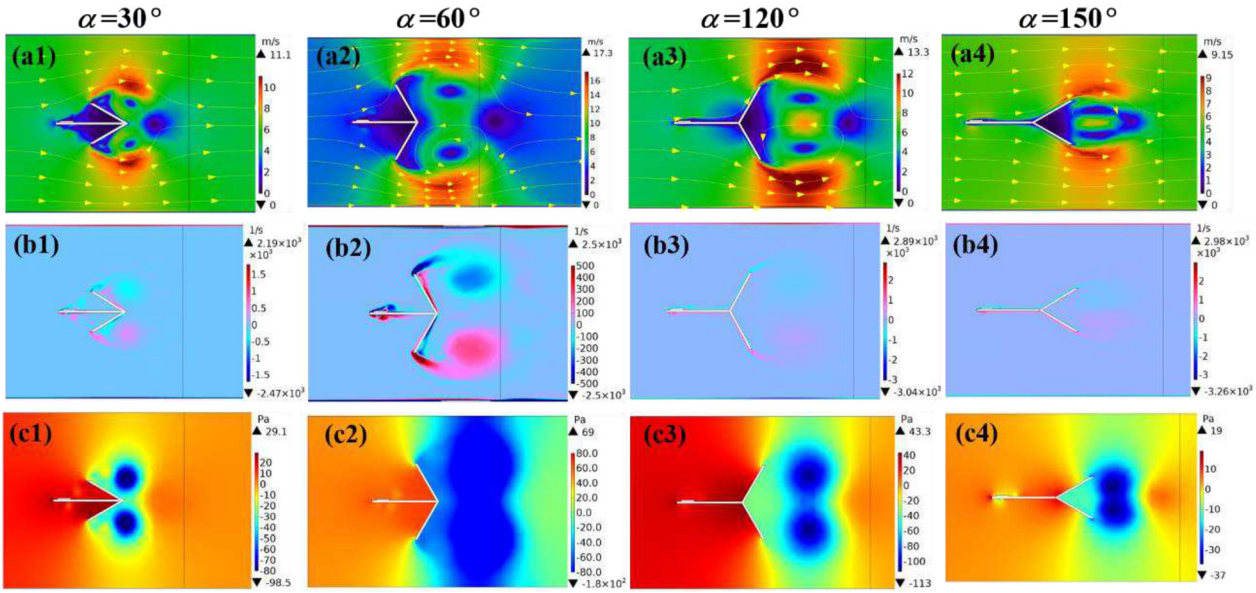

FIG. 17. The simulation results of fully fluid–structure-electric coupling (a) wind velocity field, (b) vorticity magnitude distributions, and (c) pressure distributions for V-shaped PEH with various angles at a wind velocity of 5 m/s.

increases. When the wind speed is 10 m/s, the effective vortex shedding frequency of V-shaped PEH with angles of 45° and 60° can reach above 900 Hz, and angles of 30° can also reach 650 Hz, whereas the effective vortex shedding frequency of V-shaped PEH with angles of 120°, 135° and 150° can only reach below 150 Hz, and angles of 15° can only reach 200 Hz. The angle between the two wings of the V-shaped PEH, as well as the wind speed intensity, has a substantial impact on the effective vortex shedding frequency blocked by the V-shaped PEH in the flow field.

The MFC is attached to the fixed end of V-shaped PEH. When the main cantilever beam on which it is pasted is significantly deformed, the MFC can generate a higher voltage. The first five modes of vibration and natural frequencies of the V-shaped PEH with an angle of 60° and 120° are shown in Fig. 19. It is discovered from the first five vibration modes that when the natural frequency of the V-shaped PEH is at f_4 and f_5, the MFC can have a greater deformation and the output voltage is correspondingly highest. Based on the relationship in Fig. 18 between the effective vortex shedding frequency of V-shaped PEH with various angles in the flow field and wind speed intensity, it is discovered that the effective vortex shedding frequency in the flow field of the V-shaped with an angle of 60° can reach 1000 Hz, and the frequency can effectively match the fourth and fifth order natural vibration frequencies of the V-shaped PEH; thus, a higher voltage can be output accordingly. However, in the flow field of a V-shaped with an angle of 120°, the highest effective vortex shedding frequency is just 150 Hz. Because the effective vortex shedding frequency is much lower than the natural frequency of the V-shaped PEH after the second order, the output voltage value is relatively low correspondingly.

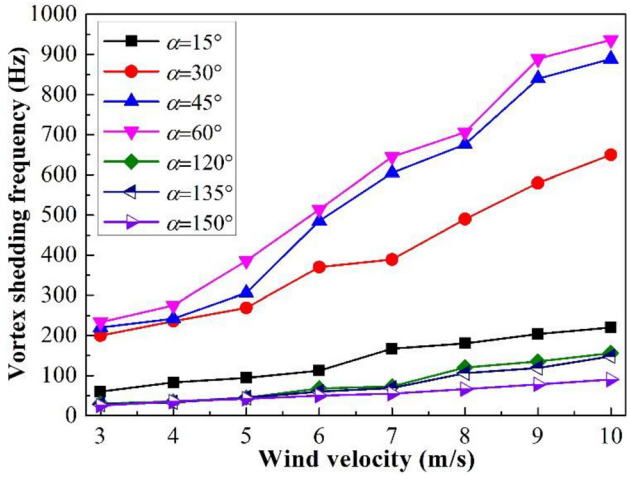

FIG. 18. The relationship between the effective vortex shedding frequency of V-shaped PEH with varied angles in the flow field and wind speed intensity.

In summary, the increase in voltage is related to the angle mainly dependent the proximity of vortex shedding frequency to beam resonance.

V. CONCLUSION

The V-shaped PEH is proposed and designed in this paper by sticking a V-shaped windward wings structure to the end of the main piezoelectric cantilever beam to transform wind energy in nature to electric energy powering for low-power electron devices. The energy harvesting experiments of the proposed V-shaped PEH are first conducted in the wind tunnel. The full fluid–solid-electric coupling simulation of the proposed V-shaped PEH model is then analyzed, which reveals the mechanism of electricity generation from the PEH vibrating in the wind flow field.

Downloaded from http://pubs.aip.org/aip/jrse/article-pdf/doi/10.1063/5.0059870/15719563/063304_1_online.pdf

Published under an exclusive license by AIP Publishing

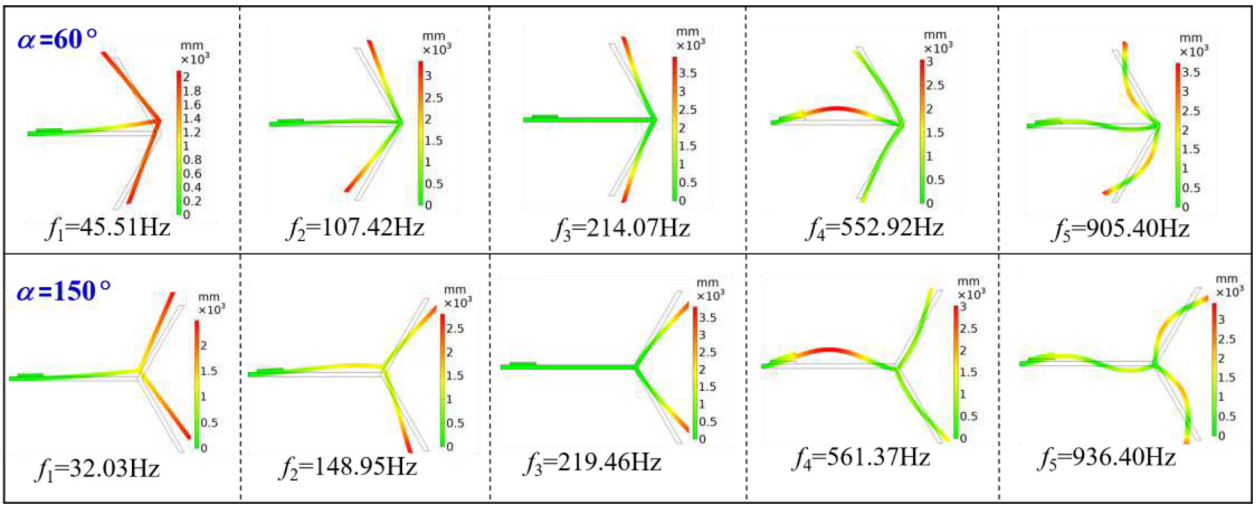

FIG. 19. The first five modes of vibration and natural frequencies of the V-shaped PEH with an angle of 60° and 120°.

Both experiment and simulation results show that the energy harvesting of the piezoelectric cantilever beam with V-shaped windward wings structure has been improved obviously in the wind flow field. The angles of windward wings in PEH have a significant influence on the output voltage. When the angle of windward wings is 60° and the wind velocity is 10 m/s, the highest peak-to-peak voltage generated by the proposed PEH reaches 96.68 V, as collected by experiments. The following $V_{AC\text{-}PP}$ is 95.20, 92.56, and 70.20 V, correspondingly generated by the proposed PEH with windward wings at angles of 45°, 30°, and 75°, respectively. When the angle is over 90°, the effective incentive influence of the flow field on the PEH significantly reduces. The voltage generated decreases distinctly and the $V_{AC\text{-}PP}$ is less than 6 V. The V-shaped PEH proposed and designed in this paper has a good performance in energy harvesting when the windward wings are in the range of rational angles, by which the voltage generated can power for electron devices with low power consumption.

ACKNOWLEDGMENTS

This work was supported by the National Natural Science Foundation of China (Nos. 11772245, 12002256, and 11572235), the Fundamental Research Funds for the Central Universities, XJTU in China (No. xjh012020014), and the Natural Science Basic Research Plan in Shaanxi Province of China (Program Nos. 2018JC-004 and 2020JQ-011). The author Qun Li gratefully acknowledges the support of K. C. Wong Education Foundation.

AUTHOR DECLARATIONS

Conflict of Interest

The authors have no conflicts to disclose.

DATA AVAILABILITY

The data that support the findings of this study are available from the corresponding author upon reasonable request. The data that support the findings of this study are available within the article.

REFERENCES

[1]B. Zhu, Y. Huang, and Y. Zhang, "Energy harvesting properties of a flapping wing with an adaptive Gurney flap," Energy **152**, 119–128 (2018).
[2]A. Abdelkefi, "Aeroelastic energy harvesting: A review," Int. J. Eng. Sci. **100**, 112–135 (2016).
[3]D. Li, Y. A. Wu, R. Da, and J. Xiang, "Energy harvesting by means of flow-induced vibrations on aerospace vehicles," Prog. Aerosp. Sci. **86**, 28–62 (2016).
[4]G. J. Sheu, S. M. Yang, and T. Lee, "Development of a low frequency electrostatic comb-drive energy harvester compatible to SoC design by CMOS process," Sens. Actuators, A **167**, 70–76 (2011).
[5]K. A. Cook-Chennault, N. Thambi, and A. M. Sastry, "Powering MEMS portable devices-a review of non-regenerative and regenerative power supply systems with special emphasis on piezoelectric energy harvesting systems," Smart Mater. Struct. **17**, 043001 (2008).
[6]Y. W. Yang, L. Y. Zhao, and L. H. Tang, "Comparative study of tip cross-sections for efficient galloping energy harvesting," Appl. Phys. Lett. **102**, 064105 (2013).
[7]Y. Qi, J. Kim, T. D. Nguyen, B. Lisko, P. K. Purohit, and M. C. McAlpine, "Enhanced piezoelectricity and stretchability in energy harvesting devices fabricated from buckled PZT ribbons," Nano Lett. **11**, 1331–1336 (2011).
[8]H. Elahi, M. Eugeni, and P. Gaudenzi, "A review on mechanisms for piezoelectric-based energy harvesters," Energies **11**, 1850 (2018).
[9]D. Vatansever, R. L. Hadimani, T. Shah, and E. Siores, "An investigation of energy harvesting from renewable sources with PVDF and PZT," Smart Mater. Struct. **20**, 055019 (2011).
[10]S. Shahab and A. Erturk, "Electrohydroelastic Euler-Bernoulli-Morison model for underwater resonant actuation of macro-fiber composite piezoelectric cantilevers," Smart Mater. Struct. **25**, 105007 (2016).
[11]D. Upadrashta and Y. W. Yang, "Experimental investigation of performance reliability of macro fiber composite for piezoelectric energy harvesting applications," Sens. Actuators, A **244**, 223–232 (2016).
[12]M. Kim, M. Hoegen, J. Dugundji, and B. L. Wardle, "Modeling and experimental verification of proof mass effects on vibration energy harvester performance," Smart Mater. Struct. **19**, 045023 (2010).
[13]A. Erturk and D. J. Inman, "An experimentally validated bimorph cantilever model for piezoelectric energy harvesting from base excitations," Smart Mater. Struct. **18**, 025009 (2009).
[14]S. Orrego, K. Shoele, A. Ruas, K. Doran, B. Caggiano, R. Mittal, and S. H. Kang, "Harvesting ambient wind energy with an inverted piezoelectric flag," Appl. Energy **194**, 212–222 (2017).

Downloaded from http://pubs.aip.org/aip/jrse/article-pdf/doi/10.1063/5.0059870/15719563/063304_1_online.pdf

Published under an exclusive license by AIP Publishing

[15]J. J. Liu, H. Zuo, W. Xia, Y. J. Luo, D. Yao, Y. J. Chen, K. Wang, and Q. Li, "Wind energy harvesting using piezoelectric macro fiber composites based on flutter mode," Microelectron. Eng. **231**, 111333 (2020).
[16]L. B. Zhang, A. Abdelkefi, H. L. Dai, R. Naseer, and L. Wang, "Design and experimental analysis of broadband energy harvesting from vortex-induced vibrations," J. Sound Vib. **408**, 210–219 (2017).
[17]R. Naseer, H. L. Dai, A. Abdelkefi, and L. Wang, "Piezomagnetoelastic energy harvesting from vortex-induced vibrations using monostable characteristics," Appl. Energy **203**, 142–153 (2017).
[18]A. H. Alhadidi and M. F. Daqaq, "A broadband bi-stable flow energy harvester based on the wake-galloping phenomenon," Appl. Phys. Lett. **109**, 033904 (2016).
[19]A. Bibo, A. H. Alhadidi, and M. F. Daqaq, "Exploiting a nonlinear restoring force to improve the performance of flow energy harvesters," J. Appl. Phys. **117**, 045103 (2015).
[20]A. Abdelkefi, L. M. Scanlon, E. McDowell, and M. R. Hajj, "Performance enhancement of piezoelectric energy harvesters from wake galloping," Appl. Phys. Lett. **103**, 033903 (2013).
[21]G. Hu, K. T. Tse, K. C. S. Kwok, J. Song, and Y. Lyu, "Experimental investigation on the efficiency of circular cylinder-based wind energy harvester with different rod-shaped attachments," Appl. Phys. Lett. **109**, 193902 (2016).
[22]J. Song, G. Hu, K. T. Tse, S. W. Li, and K. C. S. Kwok, "Performance of a circular cylinder piezoelectric wind energy harvester fitted with a splitter plate," Appl. Phys. Lett. **111**, 223903 (2017).
[23]J. Sirohi and R. Mahadik, "Harvesting wind energy using a galloping piezoelectric beam," J. Vib. Acoust. **134**, 011009 (2012).
[24]L. Ding, L. Zhang, C. M. Wu, X. R. Mao, and D. Y. Jiang, "Flow induced motion and energy harvesting of bluff bodies with different cross sections," Energy Convers. Manag. **91**, 416–426 (2015).
[25]F. R. Liu, H. X. Zou, W. M. Zhang, Z. K. Peng, and G. Meng, "Y-type three-blade bluff body for wind energy harvesting," Appl. Phys. Lett. **112**, 233903 (2018).
[26]F. R. Liu, H. X. Zou, W. M. Zhang, Z. K. Peng, and G. Meng, "Fork-shaped bluff body for enhancing the performance of galloping-based wind energy harvester," Energy **183**, 92–105 (2019).
[27]D. N. Shen, J. H. Park, J. H. Noh, S. Y. Choe, S. H. Kim, H. C. Wikle, and D. J. Kim, "Micromachined PZT cantilever based on SOI structure for low frequency vibration energy harvesting," Sens. Actuators, A **154**, 103–108 (2009).
[28]M. Rezaei, R. Talebitooti, and S. Rahmanian, "Efficient energy harvesting from nonlinear vibrations of PZT beam under simultaneous resonances," Energy **182**, 369–380 (2019).
[29]B. Gusarov, E. Gusarova, B. Viala, L. Gimeno, S. Boisseau, O. Cugat, E. Vandelle, and B. Louison, "Thermal energy harvesting by piezoelectric PVDF polymer coupled with shape memory alloy," Sens. Actuators, A **243**, 175–181 (2016).
[30]S. Tiwari, A. Gaur, C. Kumar, and P. Maiti, "Enhanced piezoelectric response in nanoclay induced electrospun PVDF nanofibers for energy harvesting," Energy **171**, 485–492 (2019).
[31]S. Bairagi and S. W. Ali, "Flexible lead-free PVDF/SM-KNN electrospun nanocomposite based piezoelectric materials: Significant enhancement of energy harvesting efficiency of the nanogenerator," Energy **198**, 117385 (2020).
[32]R. B. Williams, B. W. Grimsley, D. J. Inman, and W. K. Wilkie, "Manufacturing and mechanics-based characterization of macro fiber composite actuators," ASME International Mechanical Engineering Congress and Exposition (2002).
[33]M. Peddigari, G. T. Hwang, and J. Ryu, "A comparison study of fatigue behavior of hard and soft piezoelectric single crystal macro-fiber composites for vibration energy harvesting," Sensors **19**, 2196 (2019).
[34]A. Pandey and A. Arockiarajan, "Performance studies on macro fiber composite (MFC) under thermal condition using Kirchhoff and Mindlin plate theories," Int. J. Mech. Sci. **130**, 416–425 (2017).
[35]T. Kashiwao, I. Izadgoshasb, Y. Y. Lim, and M. Deguchi, "Optimization of rectifier circuits for a vibration energy harvesting system using a macro-fiber composite piezoelectric element," Microelectron. J. **54**, 109–115 (2016).
[36]G. L. Pankanin, "Experimental and theoretical investigations concerning the influence of stagnation region on Karman vortex shedding," *Proceedings IEEE Instrumentation and Measurement Technology Conference* (IEEE, 2007), pp. 695–700.

Downloaded from http://pubs.aip.org/aip/jrse/article-pdf/doi/10.1063/5.0059870/15719563/063304_1_online.pdf

Published under an exclusive license by AIP Publishing